Available online at www.sciencedirect.com
SCIENCE DIRECT®
Journal of Solid State Chemistry 178 (2005) 2766–2777
JOURNAL OF SOLID STATE CHEMISTRY
www.elsevier.com/locate/jssc

Synthesis of [Zn–Al–CO_3] layered double hydroxides by a coprecipitation method under steady-state conditions

Z. Chang[a,b], D.G. Evans[a], X. Duan[a], C. Vial[c], J. Ghanbaja[d], V. Prevot[b], M. de Roy[b,*], C. Forano[b]

[a] *Ministry of Education Key Laboratory of Science and Technology of Controllable Chemical Reactions, Beijing University of Chemical Technology, Beijing 100029, China*
[b] *Laboratoire des Matériaux Inorganiques, UMR CNRS 6002, Université Blaise Pascal, 24 avenue des Landais, 63177 Aubière, France*
[c] *Ecole Nationale Supérieure de Chimie de Clermont-Ferrand, 24 avenue des Landais, 63177 Aubière, France*
[d] *Service Commun de Microscopie Electronique à Transmission, Faculté des Sciences, Université H. Poincaré-Nancy I, 54506 Vandoeuvre, Nancy, France*

Received 6 May 2005; received in revised form 14 June 2005; accepted 16 June 2005
Available online 27 July 2005

Abstract

A continuous co-precipitation method under steady-state conditions has been investigated for the preparation of nanometer-size layered double hydroxide (LDH) particles using $Zn_2Al(OH)_6(CO_3)_{0.5}\cdot 2H_2O$ as a prototype. The objective was to shorten the preparation time by working without an aging step, using a short and controlled residence time in order to maintain a constant supersaturation level in the reactor and constant particle properties in the exit stream over time. The effects of varying the operating conditions on the structural and textural properties of the LDHs have been studied, including total cation concentration, solvent, residence time, pH and intercalation anion. The products have been characterized using ICP, XRD, FTIR, BET, SEM and TEM. The LDHs prepared by the continuous coprecipitation method have a poorer crystallinity and lower crystallite sizes than those synthesized by the conventional batch method. The results have shown that increasing either cation concentration or the fraction of monoethylene glycol (MEG) in MEG/H_2O mixtures up to 80% (v/v) affect salt solubility and supersaturation, which gives rise to smaller crystallites, larger surface areas and more amorphous compounds. This increase is however limited by the precipitation of zinc and aluminum hydroxides occurring around a total cation concentration of 3.0×10^{-1} M in pure water and 3.0×10^{-2} M in H_2O/EtOH mixtures. Crystallite size increases with residence time, suggesting a precipitation process controlled by growth. Finally, the continuous coprecipitation method under steady-state conditions has been shown to be a promising alternative to the traditional coprecipitation technique in either pure water or mixed H_2O/MEG solvents.

Keywords: LDH nanoparticles; Controlled precipitation; Steady-state conditions

1. Introduction

Layered double hydroxides (LDHs) constitute a family of lamellar solids characterized [1–6] by the general formula $[M_{1-x}^{II}M_x^{III}(OH)_2][A^{n}_{x/n}{}^{-}\cdot mH_2O]$. Their structure [7–11] is based on brucite-like layers in which divalent cations (M^{II}), including Co^{2+}, Cu^{2+}, Fe^{2+}, Mg^{2+}, Mn^{2+}, Ni^{2+} or Zn^{2+}, are partially substituted by trivalent ones (M^{III}), such as Al^{3+}, Cr^{3+}, Fe^{3+}, Mn^{3+} or La^{3+}. The M^{II}/M^{III} molar ratio usually lies between 2 and 5. The layers, as a result, carry a positive charge, which is balanced by interlayer anions (A^{n-}) and variable amounts of interlayer water molecules. These can be simple inorganic anions [12], such as CO_3^{2-}, SO_4^{2-}, NO_3^-, F^-, Cl^- or PO_4^{3-}, but also organic anions [13–17], complex anions [18,19] and heteropolyanions [20,21]. LDHs find widespread applications in

*Corresponding author. Fax: +33 4 73 40 71 08.
E-mail address: Marie.de_Roy@univ-bpclermont.fr (M. de Roy).

0022-4596/$ - see front matter © 2005 Elsevier Inc. All rights reserved.
doi:10.1016/j.jssc.2005.06.024

many fields, including industrial catalytic processes [22], pharmaceuticals [23], polymer reinforcement [24,25] or environmental clean-up by ion exchange [26] or adsorption process [27,28]. Furthermore, calcination of LDHs (at 300–600 °C) leads to the formation of layered mixed oxides (LDOs) [2,26–30]. These are useful solid base catalysts that find potential applications in many catalytic processes, for example for the decomposition of nitrous oxides [31,32], but also hydrogenation [33], condensation [34–38] and alkylation [39] reactions or wet oxidations [40–43]. However, the properties of LDOs are strongly linked to the chemical composition and morphology of their LDH precursors because LDO surface area and porosity result mainly from the thermal stabilities of both interlayer anion and host structure, and the textural properties of the platelet-like crystallites of the LDH precursor. Because textural properties of solids are strongly influenced by the nature of the synthesis procedures, a wide range of synthetic routes for LDHs have been developed and are currently under investigation.

Although sol–gel processes [44], the urea method [45,46], the reconstruction method [47] or emulsion solution [48] techniques have been reported in the literature, the coprecipitation of inorganic salts at constant neutral or basic pH is still the most common method to synthesize LDHs [1,4,6,49]. In this method, LDHs are obtained in batch reactors, using the simultaneous dropwise addition at constant pH of aqueous solutions of an alkali and mixed M^{II}/M^{III} salts containing the desired interlayer anion if different from that in the metal salt precursor. The influence of the M^{II} and M^{III} salts, the M^{II}/M^{III} ratio and the interlayer anion on the crystallinity and morphology properties of the coprecipitated LDHs have been widely studied in the literature cited previously. A few studies have also investigated the effects of thermal treatments [50–53] or solvent composition [54]. The first drawback of this approach is that supersaturation remains always low, except locally in the region of injection points, which does not favor the formation of nanometer-size platelets of LDHs. Additionally, precipitation conditions vary from the beginning to the end of the synthesis. Therefore, differences in crystallinity over time and large crystallite size distributions are difficult to avoid. Up to now, aging constitutes the most common way to obtain more uniform particle properties. This is the reason why, if the addition procedure lasts a few hours, it is generally followed by a long aging period, from 10 to 80 h and often longer.

In this work, an alternative to the traditional technology has been developed. It consists of a continuous precipitation method under steady-state conditions. Such a technique is known to be the most satisfactory for the preparation of solid catalysts [55] because experimental parameters, such as residence time, pH, concentration and temperature can be simultaneously kept constant over time during the operation. As a result, the supersaturation level and consequently, the structural and textural properties of the solid phase in the exit stream of the reactor should not change with time, which should give constant and narrow LDH particle size distributions. As higher supersaturation levels can be achieved, this method should also lead to smaller particle sizes and higher specific surface areas, which should be advantageous in terms of enhanced catalytic activity. Additionally, continuous precipitation is easier to adapt for large-scale production. Its main drawback however is that it is more difficult to carry out on the laboratory-scale than the standard coprecipitation method, as it requires simultaneous control of two inlet feed streams and the effluent.

The aim of this study is therefore to investigate a continuous coprecipitation technique under steady-state conditions and to determine whether it constitutes a viable alternative to the standard coprecipitation technique for the preparation of nanosized LDHs particles. Using $Zn_2Al(OH)_6(CO_3)_{0.5} \cdot 2H_2O$ as a model, systematic experiments have been conducted in order to investigate the influence of operating conditions on LDH properties such as chemical composition, crystallinity, XRD and SAED patterns, IR spectra, particle size and shape. Experimental investigations include the optimization of total cation concentration in the range 3×10^{-3}–3×10^{-1} M at constant M^{II}/M^{III} ratio, residence time from 5 to 15 min and solvent composition using pure water, ethanol-water ($EtOH/H_2O$) and monoethylene glycol-water (MEG/H_2O) mixed water–organic solvents, and also a polyethylene glycol aqueous solution. The effect of varying pH between 7 and 11 and of varying the interlayer anion among carbonate and two organic anions (acetate and benzoate anions) has also been studied. Carboxylate anions and polyol solvents are expected to limit the growth by a complexation or templating effect, respectively.

2. Experimental methods

2.1. Synthesis

Experiments have been carried out in a laboratory-scale ''vortex'' reactor under steady-state conditions (Fig. 1), at atmospheric pressure and room temperature (21 ± 1 °C). The reactor consists of a cylindrical PVC tank without baffles, having a diameter of 64 mm and height of 73 mm and containing 230 mL of solution. Mixing was achieved using a magnetic stirrer that can be adequately replaced by a Rushton turbine placed in the bottom of larger tanks [56] for industrial-scale production. A constant rotational speed of 300 rpm was used

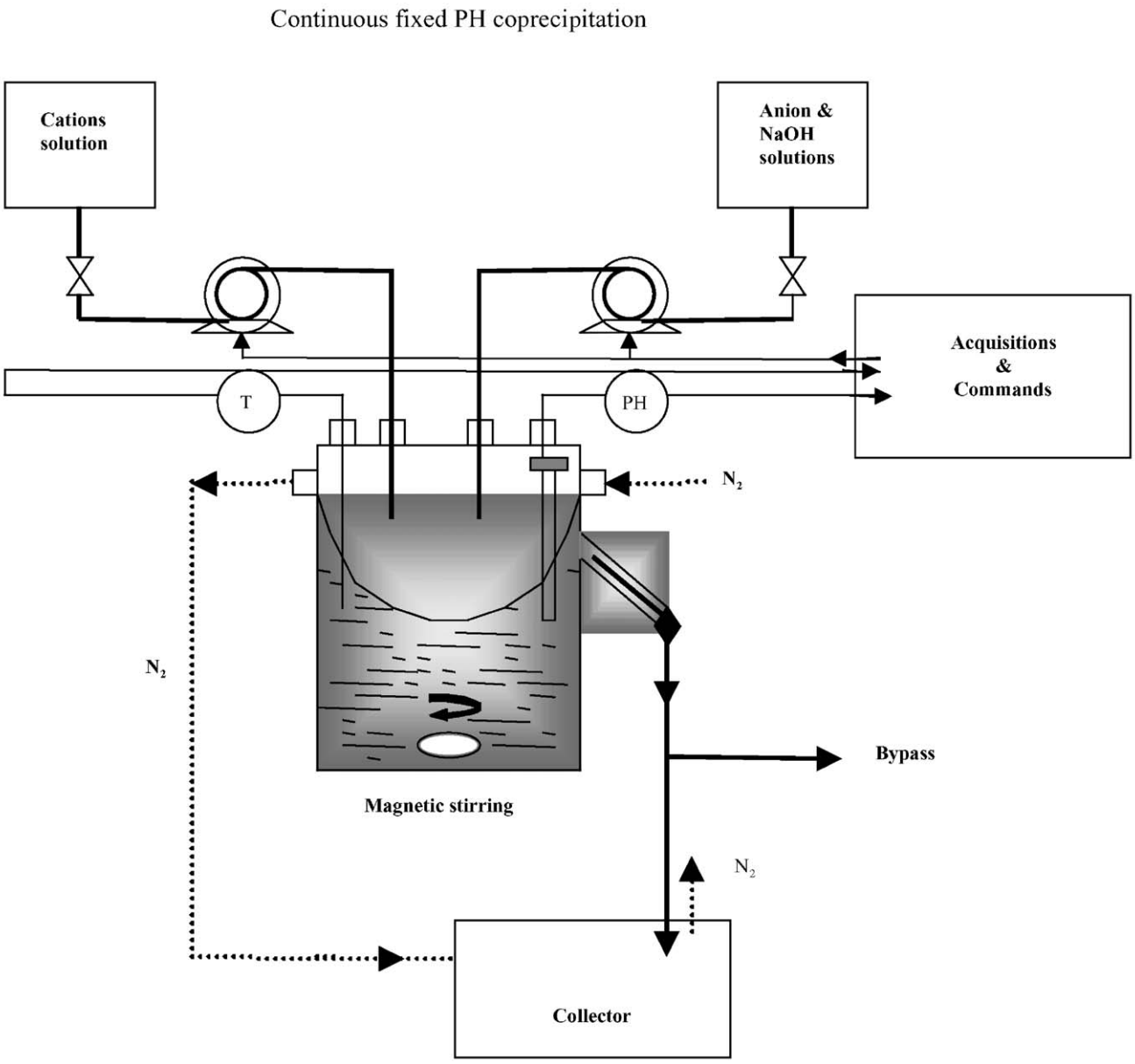

Fig. 1. Experimental setup for the continuous coprecipitation of LDH samples under steady-state conditions.

for all experiments. The rotation of the mixer without baffles generates a ''forced central vortex'' of cylindrical-conical form, which is confined by a liquid volume of annular form, denoted the ''free-vortex region''. Such a hydrodynamic mixing avoids the formation of incrustations. Its main drawback is that mixing is not rapid and residence times lower than 5 min are difficult to achieve. The reactants consist of metal cation and alkaline solutions that are supplied using two injection points located above the central zone. A pH-electrode is placed in the free vortex region for pH control during operation. Nucleation takes place essentially totally in the forced vortex region around the injection points where supersaturation is high, while the particles can undergo only growth, agglomeration and Ostwald ripening in the free vortex region where supersaturation is lower. Feed flow rates are supplied by two variable-speed peristaltic pumps connected to a PC and controlled independently using the Labworldsoft 2.6 software (*Labworld-online Gmbh,* FRG). While pH and the flow rate of the cation solution are two operating parameters directly chosen by the operator, the flow rate of the alkaline solution is adjusted automatically by the software so that the desired pH value is obtained. In this work, pH was maintained at either 7.0 ± 0.2, 9.0 ± 0.2 or 11.0 ± 0.2, while the flow rate of the cation solution was varied in order to achieve residence times between 5 and 15 min.

Table 1
Additional experiments to investigate the influence of the interlayer anion on the continuous coprecipitation technique

Sample	H_2O (% v/v)	MEG (% v/v)	EtOH (% v/v)	Residence time (min)	pH	Total cation concentration (M)	Intercalation anion concentration
W-2-9-5-Be	100	0	0	5	9	3×10^{-2}	Benzoate (10^{-1} M)
W-2-9-15-Ac	100	0	0	15	9	3×10^{-2}	Acetate (5×10^{-2} M)
W-2-9-10-Ac	100	0	0	10	9	3×10^{-2}	Acetate (10^{-1} M)
EG40-2-9-5-Ac	60	40	0	5	9	3×10^{-2}	Acetate (5×10^{-2} M)
Et40-2-9-5-Ac	60	0	40	5	9	3×10^{-2}	Acetate (5×10^{-2} M)

In the continuous coprecipitation technique, the effluent containing LDH particles, without any long-time aging, is collected continuously through the overflow pipe and stored in a tank, once steady-state conditions have been achieved in the reactor. Both the reactor and the storage tank are maintained in an inert nitrogen atmosphere during the operation in order to minimize the carbonation of the solutions due to the carbon dioxide from the atmosphere when anions other than carbonate are present in the preparation medium. Solid LDH particles are then separated from the liquid effluent using centrifugation, washed with deionized water and air-dried before storage.

All the reactants used in this work were purchased from *Acros Organics France* and used as supplied. For the preparation of the cation solutions, $ZnCl_2$ and $AlCl_3 \cdot 6H_2O$ were dissolved in either deionized water or mixed water–organic solvents including water–ethanol and water–monoethylene glycol with different volume ratios from 1:4 to 4:1 for EtOH/H_2O and MEG/H_2O. An aqueous solution of polyethylene glycol (40% w/v) was also used as a solvent. Total cation concentration, $[Zn^{2+}]+[Al^{3+}]$, has been varied from 3.0×10^{-3} to 3.0×10^{-1} M with a constant $[Zn^{2+}]/[Al^{3+}]$ ratio equal to 2 in order to form the $Zn_2Al(OH)_6(A^{n-})_{1/n} \cdot mH_2O$ LDH. The alkaline solution consists of NaOH and sodium salts of the different anions to be intercalated: carbonate, acetate or benzoate. The NaOH concentration was always equal to the total cation concentration. To favor the anion exchange reaction, intercalation anions were supplied in excess, using a 5:2 M ratio for $[CO_3^{2-}]/[Al^{3+}]$ and 5:1 for the monovalent organic anions. A set of 28 experiments was carried out with CO_3^{2-} as the interlayer anion. These experiments have been described using a four-term label, as follows: the first term represents the solvent (e.g., "W" for water, "Et40" for a 40:60 EtOH-H_2O mixed solvent and EG80 for a 80:20 MEG-H_2O solvent, "PE40" for the 40% w/v polyethylene glycol aqueous solution), the second one represents the cation concentration ("1" = 3.0×10^{-1}; "2" = 3.0×10^{-2}; "3" = 3.0×10^{-3} M), the third one corresponds to the pH value and the last one represents residence time in minutes. For example, the EG80-2-9-5 run was conducted in a 80:20 MEG/H_2O mixture with a total cation concentration of 3×10^{-2} M at a pH equal to 9 with a residence time of 5 min. Additional experiments, the aim of which was to investigate the influence of varying the intercalation anion, are summarized in Table 1.

For comparison purposes, a $Zn_2Al(OH)_6(CO_3)_{0.5} \cdot 2H_2O$ LDH was also prepared by the standard coprecipitation technique, using the slow addition of an alkaline solution (1.0 M NaOH, 0.5 M Na_2CO_3) with a metal salt solution ($[Zn^{2+}] = 0.66$ M, $[Al^{3+}] = 0.33$ M) at constant pH 1. The addition was conducted at pH 9 and took nearly 24 h. The precipitate was aged for 48 h and recovered using a similar procedure to that described for the continuous coprecipitation technique.

2.2. Characterization methods

Elemental analysis C, H and Al, Zn were carried out at the *Centre d'Analyses de Vernaison* (*CNRS*, France). The powder X-ray diffraction (XRD) patterns were recorded on a *Siemens D501* diffractometer with Cu$K\alpha$ radiation using a scanning rate of 1.2 °/min. The crystallite size of the synthesized LDHs was calculated from the line broadening of the reflections in the XRD patterns according to the Laue–Scherrer equation

$$D = K\lambda/[\Delta\varepsilon_{(2\theta)} \cos\theta], \quad (1)$$

where $\Delta\varepsilon_{(2\theta)}$ is the full width at half maximum, $K = 0.94$, is a proportionality factor related to the (00l) reflection and D is the crystallite size. The (006) reflection has been used for the determination of the full width at half maximum and the corresponding crystallite size developed along the stacking direction is noted $\varnothing 006$ in this work. The infrared transmission spectra were obtained on a *Perkin-Elmer 2000 FTIR* spectrometer using the KBr technique. The nitrogen adsorption/desorption isotherms, as preliminary experiments, were measured on a *QuantaChrome ABSORB-1* gas sorption analyzer from *Micromeritics* after outgassing the samples at 60 °C for 3 h. The pore size distribution was determined using the BJH model on the desorption branch. Scanning electron micrographs were taken on a *Cambridge Stereoscanner* electron microscope (SEM) at *CASIMIR S.A.* (France). For Transmission Electron Microscopy

(TEM), a droplet of samples resuspended in a limited volume of ethanol was layered on a Formvar-coated grids (400 Mesh) and air-dried. After deposition, the grids were examined using a *Phillips CM 20* electron microscope running at 200 kV. Some samples were analyzed by energy dispersive X-ray spectroscopy (EDX) to check their chemical composition. Selected area electron diffraction (SAED) patterns were also recorded in order to analyze qualitatively the crystallite size and the crystallinity of the samples. Transmission electron micrographs were also used to estimate the average diameter ($\varnothing$TEM) of the platelets.

3. Results and discussion

The common characteristics of the solid phases obtained using the continuous coprecipitation technique will firstly be described and summarized. The objective is to show that most of the operating conditions used with the continuous coprecipitation technique give rise to fine particles having the composition and structure of LDH phases. The effects of varying the operating conditions will be detailed, including the influence of total salt concentration, solvent, residence time, pH and intercalation anion. An attempt to explain theoretically the experimental results will be proposed. Finally, the properties of synthesized LDH compounds will be compared with those of a material obtained using the standard coprecipitation method.

3.1. Common characteristics of the prepared materials

Elemental analysis shows that all the solid phases synthesized using the continuous coprecipitation technique contain no residual Cl^- anions from the metallic salts and that they have a Zn^{2+}/Al^{3+} molar ratio close to 2, which is consistent with the ideal LDH formula $Zn2Al(OH)_6(CO_3^{2-})_{1/n}\cdot mH_2O$. Table 2 illustrates this for some typical samples (all CO_3^{2-} as the interlayer anion even if another anion is present in the preparation medium). It is however noteworthy that, for the majority of samples with CO_3^{2-} as the interlayer anion, the C/Al molar ratio is higher than the expected value, 0.5. This excess of carbon could not be caused by intercalation of organic anions coming from the preparation medium because both XRD and FTIR measurements gave evidence that they did not intercalate (Figs. 3 and 5). One possibility may be residual organic solvent or CO_3^{2-} ions adsorbed on external surfaces of the LDHs. EDX microanalysis measurements performed on five points for each sample show small disparities in the values of Zn^{2+}/Al^{3+} molar ratio, but on the whole, they are in good agreement with those obtained by ICP for all the experiments.

Transmission electron micrographs confirm that most samples clearly exhibit the characteristic LDH platelet structure with a uniform size ($\varnothing$TEM), from 80 to 200 nm, and an ill-defined shape (Fig. 2). This is also consistent with the XRD patterns that exhibit the characteristic peaks of crystalline [Zn–Al–CO_3] LDH phases. These patterns have been indexed using a hexagonal cell with rhombohedral symmetry (*R*-3*m*) where the *a* parameter represents the average intermetallic distance calculated from the position of the (110) reflection and the *c* parameter corresponds to 3 times the basal spacing (003). Similarly, the SAED patterns display ring-patterns which match well with the hexagonal structure of polycrystalline LDHs (Fig. 2), even if in comparison, only a few of the theoretical interplanar distances can be found in the electron diffraction patterns. From $\varnothing$TEM (measured from TEM micrographs) and $\varnothing$006 (Table 2) calculated from the Laue–Scherrer law, it is clear that the operating conditions, such as solvent nature, total cation concentration and residence time affect LDH properties. Fig. 3 shows a series of IR spectra of LDH compounds prepared under different conditions. The bands in the range 400–900 cm^{-1} provide evidence that the characteristic LDH network has been formed. The absorption at 450 cm^{-1} is due to the O–M–O deformation mode, while those at 580 and 780 cm^{-1} correspond to M–O stretching vibrations. The strong band observed at 1350 cm^{-1} is related to the interlayer carbonate anions

Table 2
Compositional analysis, crystallite size estimations using TEM and XRD patterns and surface areas based on nitrogen adsorption of some samples prepared using the continuous coprecipitation technique

Sample	Zn/Al molar ratio (ICP)	C/Al molar ratio	$\varnothing$006 (nm)	$\varnothing$TEM (nm)	Spec. surface area (m^2/g)
W-2-9-5	1.94	0.62	45.5	130	21.7
W-2-9-15	1.93	0.78	53.5	160	38.7
W-3-9-5	2.03	0.79	43.9	170	29.8
W-3-9-15	2.00	0.71	56.2	200	16.7
EG40-2-9-15	2.09	1.18	57.1	100	61.9
EG80-2-9-15	1.91	0.78	31.1	80	51.6
EG80-3-9-5	1.93	0.64	21.4	95	18.1
EG80-3-9-15	1.93	0.66	31.5	110	23.6
PE40-2-9-15	1.96	0.97	26.5	65	59.7

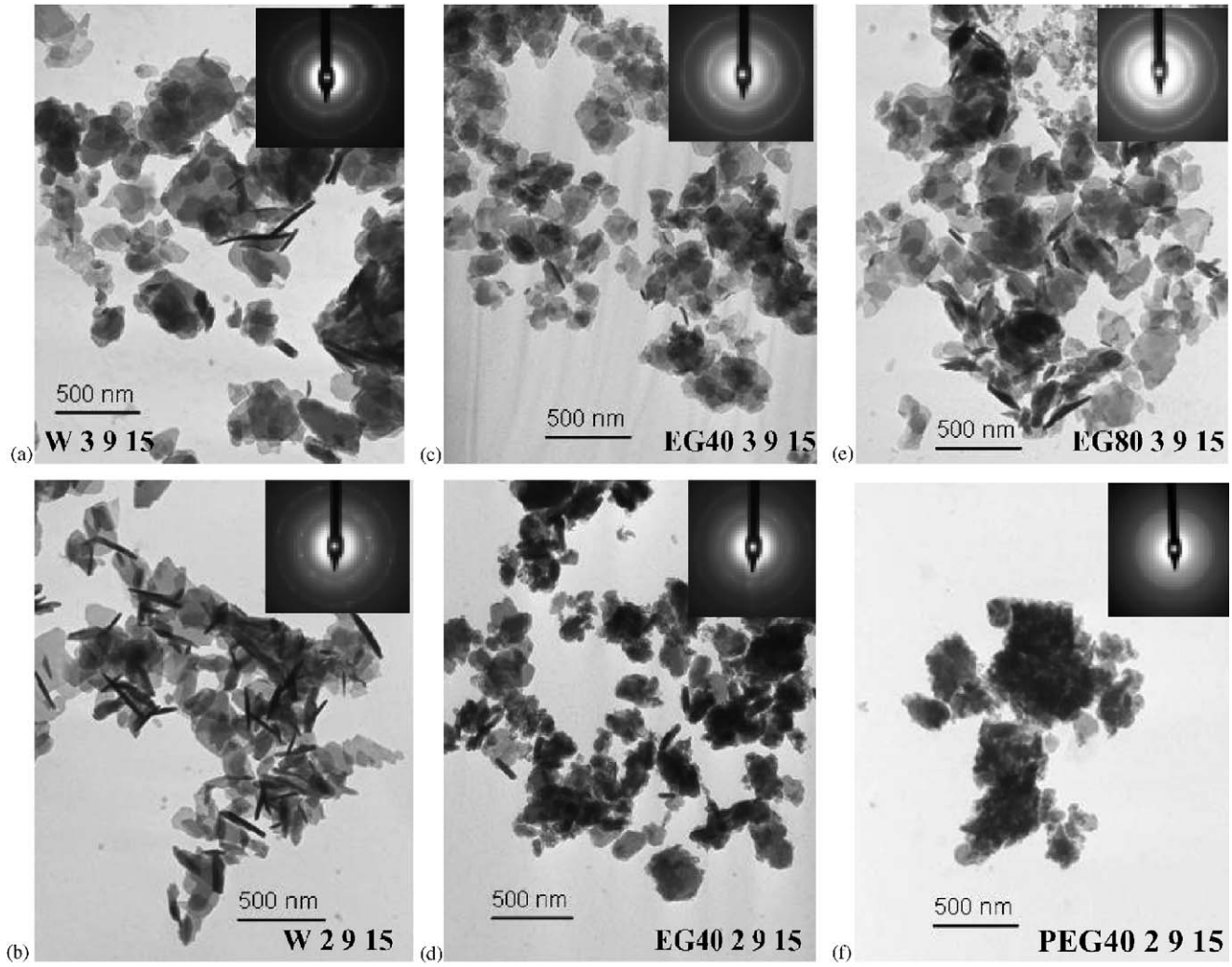

Fig. 2. TEM micrographs of LDH samples prepared at different cation concentrations in different solvents: (a) W-3-9-15, (b) W-2-9-15, (c) EG-40-3-9-15, (d) EG40-2-9-15, (e) EG80-3-9-15, (f) PEG40-2-9-15. The insets are the corresponding SAED patterns.

(ν_3). The band at 1625 cm^{-1} corresponds to the H–O–H deformation mode of intercalated water molecules and the weaker band at 640 cm^{-1} to the bending vibration mode of hydroxyl groups. It is noteworthy that for some samples, extra bands are observed around 1510 cm^{-1}, which can be ascribed to adsorbed CO_3^{2-} species. Conversely, there are no absorption bands of residual or intercalated organic solvent such as EtOH, MEG or PEG (Fig. 3(A)), suggesting that the solvents can be removed easily by the washing procedure employed. These results suggest that the high values of C/Al molar ratio reported in Table 2 are due mainly to CO_2 adsorption on the basic surface sites of the LDH during air-drying or final storage.

The measured specific surface area, corresponding to a preliminary study of textural properties, never exceeds 62 m^2/g although much higher values would be expected in view of the very low particle sizes. This is due to the sample pretreatment process used in BET analysis (degassing for 3 h at 60 °C). Indeed, in order not to further modify the textural properties of the samples we decided to use such relatively mild conditions, which may explain why the textural properties of the reported LDHs are substancially lower than those observed for most HDL materials. More investigations in conventionnal conditions will be presented in a more detailed study.

3.2. *Effect of total salt concentration*

Fig. 4 presents the powder XRD patterns of samples prepared in water as a function of total salt concentrations, 3.0×10^{-1}, 3.0×10^{-2} and 3.0×10^{-3} M, respectively. For W-1-9-10, it is worthy of note that the solid phase is rather amorphous and that it does not correspond to the LDH structure, as additional peaks can be found. Further analysis suggests that there is a mixture of LDH phases and zinc and aluminum hydroxides. This is also confirmed by IR spectra. Conversely, for lower total cation concentrations,

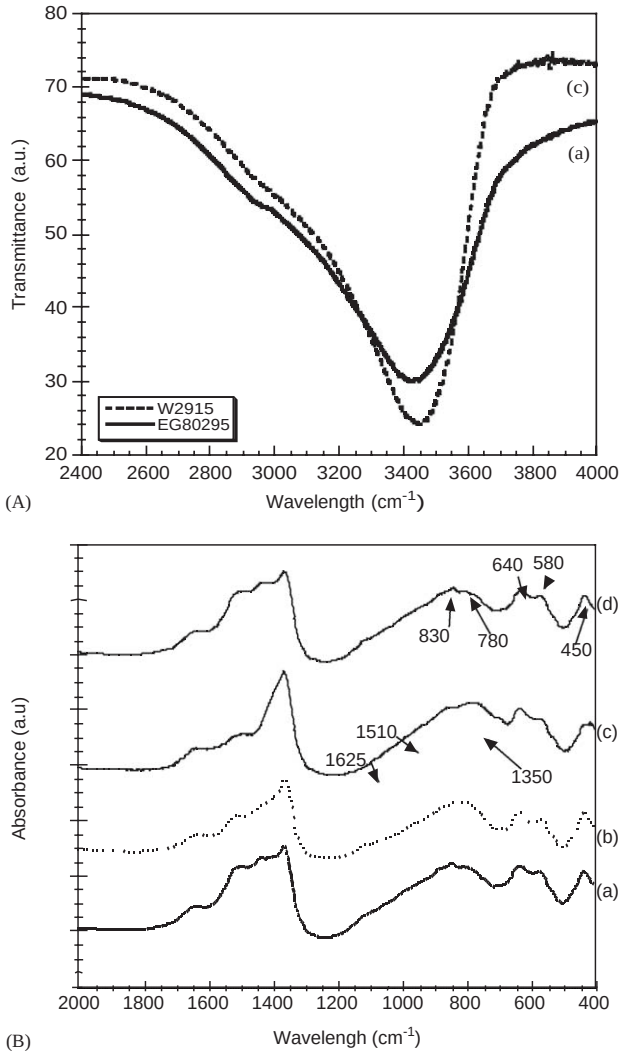

Fig. 3. FTIR spectra of LDH samples, at higher (A) and lower (B) wavenumbers: (a) EG80-2-9-15, (b) EG40-2-9-15, (c) W-2-9-15, (d) PE40-2-9-15.

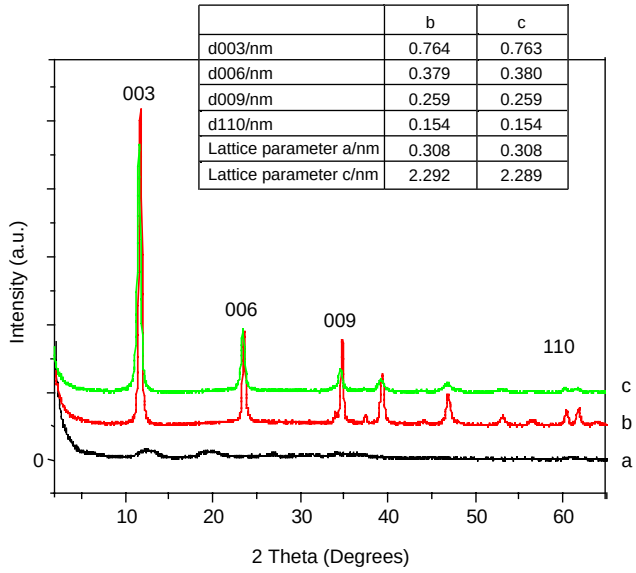

	b	c
d003/nm	0.764	0.763
d006/nm	0.379	0.380
d009/nm	0.259	0.259
d110/nm	0.154	0.154
Lattice parameter a/nm	0.308	0.308
Lattice parameter c/nm	2.292	2.289

Fig. 4. XRD patterns of samples prepared at different cation concentrations: (a) W-1-9-10, (b) W-2-9-15, (c) W-3-9-15.

LDH phases can be clearly identified by their XRD patterns. They display very little difference between 3.0×10^{-3} M (W-3-9-15) and 3.0×10^{-2} M (W-2-9-15), which shows that the particles have nearly the same size. This is in agreement with $\varnothing$006 values for W-2-9-5, W-3-9-5, W-2-9-15, and W-3-9-15 in Table 2. Furthermore, the salt concentration effect on particle shape and size is illustrated in Fig. 2 for LDHs obtained in pure water for 3.0×10^{-2} M (W-2-9-15) and 3×10^{-3} M (W-3-9-15), respectively. Transmission electron micrographs and SAED patterns confirm that the particle size decreases with increasing concentration, although this effect remains slight in pure water. However, this trend appears more clearly in MEG/H_2O mixed solvents. Only 3.0×10^{-2} and 3.0×10^{-3} M salt concentrations have been studied in this case because of the relatively low solubility of metallic salts in the water–organic solvent mixtures. XRD patterns are qualitatively similar to those observed in pure water for the same salt concentrations. SAED patterns (EG40-3-9-15 and EG40-2-9-15 in Fig. 2) and $\varnothing$TEM and $\varnothing$006 values (EG80-3-9-15 and EG80-2-9-15 in Table 2) confirm that particle size and crystallinity both decrease when the salt concentration is increased. This effect seems more pronounced in MEG/H_2O solutions, as is clearly shown by the variation of specific surface area with salt concentration given in Table 2. Specific surface areas are indeed always higher for a salt concentration of 3.0×10^{-2} M than for 3.0×10^{-3} M in MEG/H_2O mixtures and they are approximately halved when the salt concentration is reduced by a factor of 10.

3.3. *Effect of the nature of solvent*

Solvent effect is obvious through comparison of data for W-2-9-15, EG40-2-9-15, and PEG40-2-9-15 in Fig. 2. The TEM micrographs show clearly that samples with small crystallite sizes are more easily prepared in water–organic solvent mixtures and especially in the PEG solution. This trend is confirmed by SAED patterns. In water, diffraction rings are discontinuous and consist of rather sharp spots, which indicates that the particles are relatively well crystallized. Conversely, for samples prepared in the PEG solution (PE40-2-9-15), the SAED pattern consists of broad diffuse rings, typical of very small particles. The effect of preparation medium can also be observed from the XRD patterns in Fig. 5, illustrating the role of the solvent by a comparison between pure water, EtOH/H_2O, MEG/H_2O mixed solvents and PEG aqueous solutions. All the syntheses conducted in EtOH/H_2O mixtures produced amorphous samples when the salt concentration was

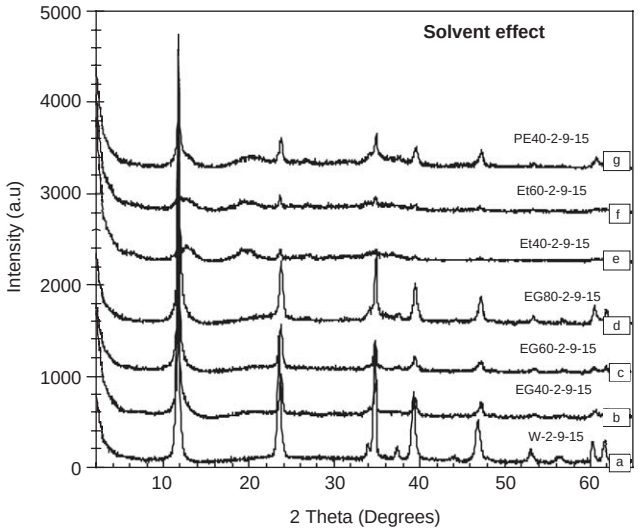

Fig. 5. XRD patterns of samples obtained in different solvents: (a) W-2-9-15, (b) EG40-2-9-15, (c) EG60-2-9-15, (d) EG80-2-9-15, (e) Et40-2-9-15, (f) Et60-2-9-15, (g) PE40-2-9-15.

3.0×10^{-2} M, except in the presence of acetate anions. This particular result will be commented on later, in Section 3.5. The solid phases obtained in EtOH/H_2O mixtures present the same XRD patterns as those obtained for W-1-9-10 (Fig. 4), and correspond to a mixture of the [Zn–Al–CO_3] LDH with zinc and aluminum hydroxides. For PE40-2-9-15, one must mention that slight quantities of such impurities can be seen in the XRD patterns, although the LDH phase is predominant (Fig. 5). TEM micrographs confirm that particles obtained in PEG solutions have the platelet structure of LDH phases (Fig. 2).

In comparison to pure water, ∅TEM (Table 2) shows a slight decrease in crystallite size in a 40:60 MEG/H_2O solvent, while ∅TEM and ∅006 (Table 2) confirm that this decrease is more significant in the 80:20 MEG/H_2O solvent mixture. The TEM micrographs for LDHs obtained in pure water, 40:60 MEG/H_2O and 80:20 MEG/H_2O as solvents illustrate the influence of the preparation medium on the shape and level of agglomeration of the particles (Fig. 2). It is noteworthy that in 80:20 MEG/H_2O mixtures, the particles are more uniform, regular and easier to disperse in comparison with those obtained in the 40:60 MEG/H_2O solution and pure water. It appears that precipitation conditions with one of the solvents as the major phase (80% or 100%) favors a higher homogeneity of particle size and a better crystallization than when a highly heterogeneous medium is used (40/60 for instance) (see Fig. 5(a)–(d)). The samples prepared in the PEG solution and in the 80:20 MEG/H_2O have the smallest particle size according to ∅006. However, the SAED patterns of PE40-2-9-15, consisting of broader diffuse rings (Fig. 2), and its ∅TEM value tend to suggest that the experimental conditions for PE40-2-9-15 give the smallest particle sizes (Table 2).

3.4. Effect of residence time

Two typical residence times have been systematically tested, 5 and 15 min, while other values, such as 10 min, have been studied for a few samples in order to check the evolution of LDH properties as a function of residence time. Both the platelet size and the coherence of the platelet organization increase gradually with residence time in water. Fig. 2 confirms the evolution of platelet size with residence time, both in deionized water and MEG/H_2O mixtures, which is also shown by the values of ∅006 and ∅TEM in Table 2. These data clearly show that the effect of residence time is more pronounced in MEG/H_2O solvents than in pure water. Decreasing the residence time and increasing the amount of organic molecules in the mixed solvents also have a similar effect on crystallinity. Rather amorphous particles are observed for EG80-3-9-5, while crystallinity increases both with residence time and water fraction in the solvent. However, it is obvious that the effect of residence time is quantitatively less significant than that of solvent or salt concentration. This is shown, for example, by the slight variation of the specific surface area in Table 2 with residence time.

3.5. Effects of pH and anions present in preparation medium

XRD patterns of samples prepared at different pH values are shown in Fig. 6. They show that LDH phases

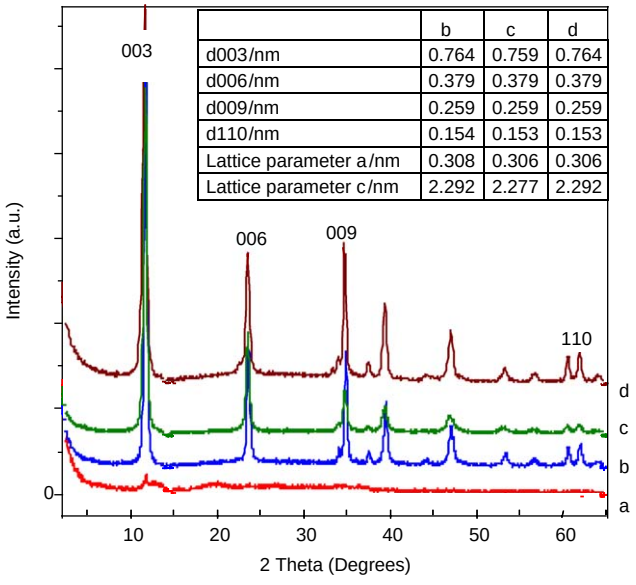

	b	c	d
d003/nm	0.764	0.759	0.764
d006/nm	0.379	0.379	0.379
d009/nm	0.259	0.259	0.259
d110/nm	0.154	0.153	0.153
Lattice parameter a/nm	0.308	0.306	0.306
Lattice parameter c/nm	2.292	2.277	2.292

Fig. 6. XRD patterns of LDH samples prepared at different pH values: (a) W-2-7-10, (b) W-2-9-15, (c) W-2-11-10, (d) standard method (pH 9).

are obviously not obtained at pH 7, while similar results are observed at pH 9 and 11 when total cation concentration is 3.0×10^{-2} M. It should be noted that [Zn_2Al–CO_3] LDHs particles are readily prepared using standard coprecipitation methods at pH values as low as 7.0. But in such conditions, long aging periods are generally used and thermodynamically stable solids are then obtained. In steady-state conditions, with short contact times such as 5 to 15 min, we must presume that the kinetic product is first prepared at pH 7 and is not allowed to transform to an LDH. Compositional analysis, FTIR spectra and XRD patterns confirm that W-2-11-10 and W-2-9-15 have nearly the same characteristics, for example $\varnothing$006 values around 55 nm. The only difference between them is apparent from Fig. 6 where the presence of less organized platelets in the SEM micrographs for W-2-11-10 probably denotes more rapid kinetics when the pH is 11.

In additional experiments with other anions, XRD spacing and FTIR spectra have confirmed that the characteristic bands of either acetate or benzoate are present in the particles formed as reported in Table 1. The organic anions appear to give smaller crystallites in pure water than carbonate-based LDHs, as $\varnothing$006 is around 27 nm for W-2-9-5-Be and 23 nm for W-2-9-10-Ac, while $\varnothing$006 is 45 nm and 53 nm for W-2-9-5 and W-2-9-15, respectively (Table 2). A similar result has been obtained in 40:60 MEG/H_2O mixtures for which $\varnothing$006 decreases from 57 nm in EG40-2-9-15 to 28 nm in EG40-2-9-5-Ac. Although any attempt to prepare LDH phases in EtOH/H_2O mixtures using a 3.0×10^{-2} M total salt concentration was unsuccessful, unexpectedly only the presence of acetate anions in conditions similar to those for carbonate anions seems to permit the precipitation of LDH phases (sample Et40-2-9-5-Ac). This confirms that the anion plays an active role in the mechanism of LDH formation. Moreover, acetate addition to 40:60 MEG/H_2O mixtures gives rise to the formation of LDH particles with a much more pronounced agglomeration level and a higher degree of crystallinity (Fig. 7). Similar trends have been observed in the SEM micrographs, especially for EG40-2-9-5-Ac and Et40-2-9-5-Ac. As a result, it can be concluded that the acetate and benzoate anions favor the synthesis of smaller crystallites, but form bigger particles due to the large amount of agglomeration and present finally a higher degree of crystallinity than carbonate-based LDHs.

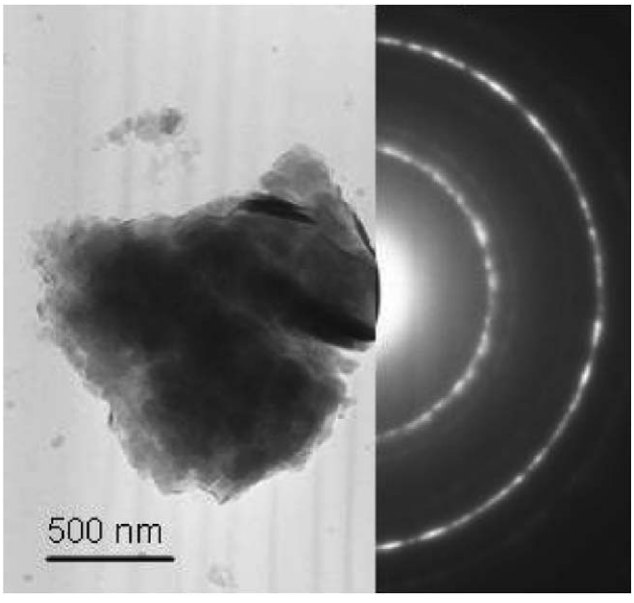

Fig. 7. TEM micrograph and SAED pattern of LDH sample EG40-2-9-5-Ac prepared in the presence of acetate anions.

3.6. Discussion

Supersaturation constitutes the thermodynamic driving force for all precipitation and crystallization processes. It is usually defined as the difference (“absolute supersaturation”) or the ratio (“supersaturation ratio”) between the concentration of and the solubility of a chemical compound. Using the reaction quotient (Q_R) concept [57], the classical expression of the chemical potential (μ) as a function of molar fractions x_i and activity coefficients γ_i can be written as follows:

$$\mu = \mu_0 + RT \sum_i \log \dot{x}_i\dot{\gamma}_i = \mu_0 + RT \log \dot{Q}_R$$

$$= RT \log \dot{Q}_R/K_S,$$

where K_S is the solubility constant. By introducing the supersaturation ratio (S), one obtains therefore

$$S = Q_R/K_S \text{ and } \mu = RT \log \dot{S}.$$

In the classical coprecipitation technique, the dropwise addition of the alkaline solution is used to achieve $Q_R > K_S$ ($S > 1$), but the cation consumption decreases in the vessel during precipitation, which correspond to a decrease in S and Q_R over time. As a result, Q_R tends to K_S during precipitation and the properties of crystals formed by chemical reaction may change over time. Conversely, in steady-state method, the simultaneous addition of the cation and the alkaline solutions ensures a better control on supersaturation level: the supersaturation ratio is constant over time and S can be adjusted precisely using the flow rates of the reactants feeds. In both cases, supersaturation governs the kinetics of crystallite nucleation and growth, but it may also affect the mechanisms of nucleation and growth. While these mechanisms have been widely described in the literature for simple precipitation processes, the more complex field of coprecipitation remains relatively explored, although one can assume that the general rules of simple precipitation can be applied. The quantification of these phenomena for coprecipitation

remains a problem to be tackled in the future however. As a rule of thumb, one can assume [58–61] that nucleation rate, r_N, is related to supersaturation, S, as follows:

$$r_N = A \exp[-B/(\log S)^2], \quad (2)$$

while the growth rate G, is expressed as

$$G = CS^n, \quad (3)$$

where A, B, C are constant parameters and $1<n<2$ when $S>1$. From these equations, it can be concluded that low supersaturation favors growth and Ostwald ripening, thus leading to large crystallites and rather well-crystallized compounds, whereas high supersaturation favors nucleation and agglomeration, producing small crystallites and more amorphous materials [62,63]. This explains and justifies the influence of the solvent and the total salt concentration described above for a fixed Zn^{2+}/Al^{3+} ratio. Supersaturation increases with total salt concentration, which corresponds to smaller crystallites exhibiting a more pronounced level of agglomeration and larger specific surface areas. Similarly, supersaturation increases in water–organic mixed solvents due to the lower solubility of metallic salts in such mixtures, which leads also to similar effects on crystallite size and crystallinity. This trend is however limited to a total salt concentration of 3.0×10^{-1} M in pure water, as the precipitation of aluminum and zinc hydroxides begins to compete with that of LDH compounds. This is confirmed in EtOH/H_2O mixtures at a lower salt concentration, 3.0×10^{-2} M, probably corresponding to a similar supersaturation level. While precipitation of LDH phases is difficult in EtOH/H_2O mixtures, it is easy in MEG/H_2O mixed solvents and, to a lesser extent, in PEG aqueous solutions, which indicates that the effect of solvent is not limited to a change in supersaturation. Increasing MEG content induces an increase in viscosity and in PEG solutions it is even higher. Viscosity affects mixing, which acts on the local supersaturation and seems to favor the precipitation of compounds requiring a lower supersaturation level (i.e., the LDH phase) as long as mixing is sufficiently good. Additionally, viscosity is known to have a strongly negative effect on growth rate, as it decreases ion diffusivity near the surface of already formed crystallites. This explains why residence time has a greater impact in viscous solvents. As nucleation seems to be rapid, residence time affects only particle size by controlling growth, especially in the free vortex zone where supersaturation is low. In pure water, growth is so rapid that the differences in crystallite size remains small between 5 and 15 min, which is not the case in viscous media, such as 80:20 MEG/H_2O and PEG solutions. If chloride is exchanged easily by carbonate, acetate or benzoate anions, the influence of the intercalation anion is probably the most difficult to interpret. Acetate anions have been found to favor LDH phases over simple hydroxides in EtOH/H_2O mixtures. This could be due to the complexing properties of acetate, which may interact with the metallic cations in solution since this in accordance with the large level of agglomeration observed in this case. It is also clear that the intercalation reaction cannot be considered independently from the formation of the pillared LDH structure in the continuous coprecipitation technique. This is a very important point that highlights another difference between the conventional and our novel LDH synthesis technique. In the former case, the interlayer anion is usually added along with the alkaline solution, and as a result its concentration changes with time in the reactor and the kinetics of the LDH formation and intercalation reaction may differ. For example, the [Zn–Al–Cl] LDH could be formed in the initial period when there is a large excess of chloride in solution and transform gradually into [Zn–Al–CO_3] when the amount of CO_3^{2-} in the reactor is sufficiently high. This is not the case in the continuous technique for which the ratio between the anion of the metallic salts (here, Cl^-) and the intercalation anion is constant over time. So, LDH formation and intercalation reaction occur simultaneously, which reinforces the role of the interlayer anion. It is therefore possible that the intercalation reaction could slow down the whole process of LDH precipitation, which would explain why smaller particles are obtained with acetate and benzoate.

3.7. Comparison with the standard preparation method

From the preceding results, it is clear that the continuous coprecipitation method under steady-state conditions constitutes a versatile tool for producing nanometer-platelet [Zn–AlCO_3] LDH structures in water or organic-water mixed solvents, such as MEG/H_2O or PEG aqueous solutions when the total cation concentration is 3.0×10^{-2} M or lower. Comparison with samples obtained using the traditional method in pure water with a long aging period shows that batch synthesis provides large platelets ($\varnothing 006 \approx 81$ nm) with a high degree of crystallinity and a low specific surface area, only 6.01 m^2/g. TEM confirms the change in particle size and shows that these platelets can be more difficult to disperse than those obtained with the continuous method. To obtain the same quantity of LDH compounds in reactors of similar volumes using either the continuous (total salt concentration: 3.0×10^{-2} M) or the batch process (total salt concentration: 1.0 M), the preparation time can be decreased from 10–70 to 3–9 h in pure water. The benefit is even higher in MEG/H_2O mixtures or PEG aqueous solutions because of the lower solubility of metallic salts in these media, which particularly affects the standard method. Additionally, the new procedure has the advantage of

keeping constant simultaneously all the experimental parameters, such as residence time, pH and supersaturation, thus allowing a better control over LDH phase properties, such as particle size and crystallinity. As this can be easily adapted for large-scale production, it appears therefore to be a promising alternative to the traditional technology for the manufacture of nanometer-size crystallized LDHs.

4. Conclusions

In this work, it has been shown that nanometer-size standard LDH materials characterized by narrow size distributions and uniform platelet configurations can be easily synthesized using a novel continuous coprecipitation technique under steady-state conditions. This presents many advantages over the standard technique. First, an aging step is not necessary, which reduces the preparation time considerably, but it also enables a better control over LDH characteristics, such as the size and shape of the platelets, their agglomeration level and their specific surface area. The effects of preparation conditions on the structural and textural properties of LDHs have been studied in detail, using [Zn–Al–CO_3] LDH as an example. Of the different parameters investigated, the total metallic cation concentration and the use of mixed water–organic solvents have been shown to have the most significant influence on LDH properties. These effects have been explained primarily through a change in supersaturation, but the role of the viscosity of the preparation medium has also been emphasized. A total salt concentration of 3.0×10^{-2} M has been shown to be optimal, either in pure water or mixed solvents based on MEG and PEG, for the production of large quantities of small LDH particles. To a lesser extent, residence time can also be used to adjust the properties of LDH materials, as it has been shown to affect mainly particle growth. The role of the interlayer anion has also been highlighted, although it remains difficult to explain. Further work is still needed to investigate the thermal behavior of the LDH phases produced by the continuous coprecipitation technique, especially in respect of formation of LDOs, but also to confirm the results in a pilot-scale reactor for future application in large-scale productions.

References

[1] V. Rives (Ed.), Layered Double Hydroxides: Present and Future, Nova Science Publishers, New York, 2001.
[2] V. Rives, Mater. Chem. Phys. 75 (2002) 19.
[3] F. Malherbe, C. Forano, J.P. Besse, in: Book of Abstracts of 213th ACS National Meeting, San Francisco, 1997, April 13–17.
[4] F. Cavani, F. Trifiro, A. Vaccari, Catal. Today 11 (1991) 173.
[5] F. Trifiro, A. Vaccari, in: G. Alberti, T. Bein (Eds.), Comprehensive Supramolecular Chemistry, Pergamon, Elmsford, New York, 1996, p. 296.
[6] A. de Roy, C. Forano, K. El Malki, J.P. Besse, in: M.L. Ocelli, H.E. Robson (Eds.), Synthesis of Microporous Materials, vol. 2, Van Nostrand Reinhold, New York, 1992, p. 108.
[7] F. Malherbe, J.P. Besse, J. Solid State Chem. 155 (2000) 332.
[8] D. Tichit, N. Das, B. Coq, R. Durand, Chem. Mater. 14 (2002) 1530.
[9] U. Olsbye, D. Akporiaye, E. Rytter, M. Rønnekleiv, E. Tangstad, Appl. Catal. A: Gen. 224 (2002) 39.
[10] S.P. Newman, W. Jones, New J. Chem. 22 (1998) 105.
[11] S.P. Newman, W. Jones, in: Supramolecular Organisation and Materials Design, Cambridge University Press, Cambridge, UK, 2001, p. 295.
[12] A. Ookubo, K. Ooi, H. Hayashi, Langmuir 9 (1993) 50.
[13] L. Raki, D.G. Rancourt, C. Detellier, Chem. Mater. 7 (1995) 221.
[14] N.T. Whilton, P.J. Vickers, S. Mann, J. Mater. Chem. 7 (1997) 1623.
[15] C.P. Kelkar, A.A. Schutz, Microporous Mater. 1 (1993) 33.
[16] K.R. Franklin, E. Lee, C.C. Nunn, J. Mater. Chem. 5 (1995) 565.
[17] S. Carlino, Solid State Ionics 98 (1997) 73.
[18] H.C.B. Hansen, C.B. Koch, Clays Clay Miner. 42 (1994) 170.
[19] E. Lopez-Salinas, Y. Ono, Microporous Mater. 10 (1997) 163.
[20] E.W. Serwicka, P. Nowak, K. Bahranowski, W. Jones, F. Kooli, J. Mater. Chem. 7 (1997) 1937.
[21] T. Kwon, G.A. Tsigdinos, T.J. Pinnavaia, J. Am. Chem. Soc. 110 (1988) 3653.
[22] J. Carpentier, J.F. Lemonier, S. Siffert, E.A. Zhilinskaya, A. Aboukaïs, Appl. Catal. 234 (2002) 91.
[23] A. Ookubo, K. Ooi, H. Hayashi, J. Pharm Sci. 40 (1994) 145.
[24] T.J. Pinnavaia, G.W. Beall, in: Polymer-Clay Nanocomposites, Wiley, West Sussex, 2000.
[25] F. Leroux, J.P. Besse, Chem. Mater. 13 (2001) 3507.
[26] V. Rives, M.A. Ulibarri, Coordin. Chem. Rev. 181 (1999) 61.
[27] J. Inacio, C. Taviot-Gueho, C. Forano, J.P. Besse, Appl. Clay Sci. 18 (2001) 255.
[28] Y. You, H. Zhao, G.F. Vance, Appl. Clay Sci. 21 (2002) 217.
[29] E.L.M. Moujahid, J. Inacio, J.P. Besse, F. Leroux, Microporous Mesoporous Mater. 57 (2001) 195.
[30] F. Basile, A. Vaccari, in: Layered Double Hydroxides: Present and Future, Nova Sciences Publishers, New York, 2001 (Chapter 10).
[31] R. Drago, K. Jurczyk, N. Kob, Appl. Catal. B: Environ. 13 (1997) 69.
[32] H. Dandl, G. Emig, Appl. Catal. A: Gen. 168 (1998) 261.
[33] F. Medina, D. Tichit, B. Coq, B.T. Dung, J. Catal. 167 (1999) 145.
[34] E. Dimitriu, V. Julea, C. Chelaru, C. Catrinescu, D. Tichit, R. Durand, Appl. Catal. A: Gen. 178 (1999) 145.
[35] A. Corma, S. Iborra, S. Miquel, J. Primo, J. Catal. 173 (1998) 315.
[36] A. Guida, M.H. Lhouty, D. Tichit, F. Figueras, P. Geneste, Appl. Catal. A: Gen. 164 (1997) 251.
[37] M.A. Aramendía, V. Borau, C. Jiménez, J.M. Marinas, J.R. Ruiz, F.J. Urbano, Microporous Mesoporous Mater. 29 (1999) 319.
[38] D. Tichit, M.N. Bennami, F. Figueras, J.R. Ruiz, Langmuir 14 (1998) 2086.
[39] S. Velu, C.S. Swamy, Appl. Catal. A: Gen. 199 (1994) 241.
[40] S.V. Christoskova, M. Stoyanova, M. Georgieva, Appl. Catal. A: Gen. 208 (2001) 243.
[41] A. Pintar, J. Levec, Chem. Eng. Sci. 47 (1992) 2395.
[42] J. Barrault, C. Bouchoule, K. Echachoui, N. Frini-Srasra, M. Trabelsi, F. Bergaya, Appl. Catal. B: Environ. 15 (1998) 269.
[43] S. Valange, Z. Gabelica, M. Abdellaoui, J.M. Clacens, J. Barrault, Microporous Mesoporous Mater. 30 (1999) 177.
[44] T. Lopez, P. Bosh, E. Ramos, R. Gomez, O. Novaro, D. Acosta, F. Figueras, Langmuir 12 (1996) 189.

[45] M. Ogawa, H. Kaiho, Langmuir 18 (2002) 4240.
[46] M. Adachi-Pagano, C. Forano, J.P. Besse, J. Mater. Chem. 13 (2003) 1988.
[47] F. Kooli, C. Depège, A. Ennaqadi, A. de Roy, J.P. Besse, Clays Clay Minerals 45 (1997) 92.
[48] J. He, B. Li, D.G. Evans, X. Duan, Colloids Surf. A: Physicochem. Eng. Aspects 251 (1999) 191.
[49] J.W. Boclair, P.S. Braterman, Chem. Mater. 11 (1999) 298.
[50] F. Basile, G. Fornasari, M. Gazzano, A. Vaccari, Appl. Clay Sci. 16 (2000) 185.
[51] F.M. Labajos, V. Rives, M.A. Ulibarri, J. Mater. Sci. 27 (1992) 1546.
[52] S. Möhmel, I. Kurzawski, D. Müller, W. Geßner, Cryst. Res. Technol. 37 (2002) 359.
[53] Y. Zhao, F. Li, R. Zhang, D.G. Evans, X. Duan, Chem. Mater. 14 (2002) 4286.
[54] F. Malherbe, C. Forano, J.P. Besse, Microporous Mater. 10 (1997) 67.
[55] Ph. Courty, Ch. Marcilly, in: G. Poncelet, P. Grange, P.A. Jacobs (Eds.), Preparation of Catalysts III, Elsevier, Amsterdam, The Netherlands, 1983, p. 485.
[56] N. Bénet, H. Muhr, E. Plasari, J.M. Rousseaux, Powder Technol. 128 (2002) 93.
[57] P. Atkins, J. de Julia, Atkins's Physical Chemistry, sevemth ed., Oxford Press, 2001.
[58] A. Mersmann, in: Crystallisation Technology Handbook, second ed., Marcel Dekker Inc., New York, USA, 2001.
[59] A.S. Myerson, in: Handbook of Industrial Crystallisation, second ed., Butterworth-Heinemann, Woburn, MA, USA, 2002.
[60] O. Söhnel, J. Garside, in: Precipitation: Basic Principles and Industrial Applications, Butterworth-Heinemann, Oxford, UK, 1992.
[61] A.G. Jones, in: Crystallisation Process Systems, Butterworth-Heinemann, London, UK, 2002.
[62] A. Mersmann, Chem. Eng. Process. 38 (1999) 345.
[63] J. Franke, A. Mersmann, Chem. Eng. Sci. 11 (1995) 1737.